

Raman Shift and Photoconductive of The Au-decorated TiO₂: Fullerene Films



Heba H. Ali*, Mazin A. Alalouisi

Department of Physics, College of Science, University of Anbar, Ramadi, IRAQ

ARTICLE INFO

Received: 21 /12 /2023
Accepted: 14 /05 /2024
Available online: 15 /01 /2025

DOI: 10.37652/juaps.2024.145487.1169

Keywords:

Fullerene, TiO₂, Raman, photoluminescence, Photoconductivity.

Copyright©Authors, 2024, College of Sciences, University of Anbar. This is an open-access article under the CC BY 4.0 license (<http://creativecommons.org/licenses/by/4.0/>).



ABSTRACT

Au-decorated fullerene:TiO₂ films were created via electrospraying at a temperature of 300 °C and a bias voltage of 5 KV. The structural properties, Raman spectra, photoluminescence (PL), and photoconductivity were studied by changing the ratio of TiO₂ to carbon. X-Ray diffraction spectra revealed changes in the distribution of C₆₀ and polymeric C₆₀ and C₇₀ structures. Raman spectra unveiled the characteristic vibrational modes of fullerenes H_g⁽¹⁾, F_g⁽¹⁾, and A_g⁽²⁾ with slight changes in the intensity and breadth of lines. The PL spectra under excitation at a wavelength of 280 nm displayed an increase in the peak intensity at approximately 562 nm without alterations in its position. The spectra resulting from excitation at a wavelength of 320 nm displayed transitions in the ultraviolet-visible region, whose locations and intensity changed depending on the percentage of TiO₂. This finding led to a modification in the optical response of the prepared films measured by $\langle R/R_0 \rangle$ as a function of the optical conductivity under irradiation at wavelengths of 200–800 nm. The optimal photoconductivity of the fullerene:TiO₂ film was 30%.

1. Introduction

Photocatalysts are materials that can accelerate a chemical reaction under light irradiation. They are widely used in various fields such as environmental remediation, energy conversion, and chemical synthesis [1]. Recently, photocatalysts have also been applied in biosensing, which is a rapidly growing field that involves the detection of biological molecules or organisms [2]. Photocatalysis is a process that involves the absorption of light by a material, leading to the generation of electron-hole pairs. These electron-hole pairs can then participate in redox reactions with adsorbed species on the surface of the photocatalyst [3]. The most commonly used photocatalyst is titanium dioxide (TiO₂), which has a wide bandgap and can absorb ultraviolet (UV) light. When TiO₂ is irradiated with UV light, it generates electron-hole pairs that can react with water or oxygen molecules to produce reactive oxygen species (ROS), such as hydroxyl radicals ($\bullet\text{OH}$) and superoxide radicals ($\bullet\text{O}_2^-$).

These ROS can then oxidize or reduce target molecules on the surface of the photocatalyst [4]. Addition to, fullerene has two interesting properties, which are the delocalized conjugated structures and electron-accepting ability. C₆₀ can efficiently promote rapid photo induced charge separation and slow charge recombination. Although the role of C₆₀ in accepting the photogenerated electrons from TiO₂ particles has been demonstrated, a few efforts are being made to utilize the unique properties of C₆₀ to increase the efficiency of photocatalysis [5]. Photocatalysis has been mostly focused on TiO₂-based photocatalysts because of their physical and chemical stability, low cost, availability, nontoxicity, and unique electronic and optical properties. However, there are still some problems to be solved to improve the photocatalytic activity of TiO₂. The high rate of electron-hole recombination in TiO₂ particles results in a low efficiency of photocatalysis. It is undeniable that further increasing the activity of TiO₂ will be of great interest to extend the practical application of the material carbon structures such as activated carbon and carbon nanotubes offer new opportunities to develop nanocomposites with unusual photocatalytic properties. Therefore, it is possible that

*Corresponding author at : Department of Physics, College of Science, University of Anbar, Ramadi, IRAQ
ORCID:<https://orcid.org/0000-0000-0000-0000>,
Tel: +964 7815358863
Email: heb21s2007@uoanbar.edu.iq

the photocatalytic activity of TiO₂ can be enhanced if fullerene is introduced into the TiO₂ photocatalyst [6].

Numerous modification methods, such as impurity doping, semiconductor coupling, and dye sensitization, have been employed to improve the efficiency and capability to utilize visible photons. A promising alternative to improving the photocatalytic property of TiO₂ is the decoration of its surface with gold nanoparticles (Au NPs). Au NPs can act as electron traps for electron-hole dissociation, which improves quantum yield. In addition, Au NPs can serve as photosensitizers that generate high-energy electrons upon surface plasmon resonance (SPR) excitation in the visible range. Therefore, the formation of hybrid materials composed of TiO₂ and Au NPs allows one to combine the attractive properties of these classes of materials. SPR is highly sensitive to the size, shape, and loading amount of noble metal NPs, which determines the photocatalysis efficiency of the composite structure [7].

Many studies discussed the enhancement of fullerenes to photosensing whether as photodetectors or photocatalysts; Vishnoi et al.[8]. synthesized nanocomposite AuNPs- coated (C₆₀ and C₇₀) thin films using the thermal co-evaporation technique to estimate the SERS and SPR. Qin et al.[9] used graphene as a layer for a C₆₀ collecting (a large-scale all-carbon hybrid film) for inherently strong and tunable UV absorption about 10⁷ A/W of photoresponsivity and a long operating time relatively. Liu et al. have enhanced a hybrid structure by introducing a fullerene n-type semiconductor hybrid into PC71BM/g-C₃N₄. This outcome was achieved through self-assembly on the surface of g-C₃N₄, which synthesized a photocatalyst in the range of 450–650 nm. This photocatalyst exhibited efficient inhibition against *E. coli* and *S. aureus* bacteria, and it demonstrated a high capability for the photocatalytic degradation of rhodamine B and tetracycline[10]. P. Bhargava et al. improved the photocatalytic activity of CC-TiO heat treated at different temperatures and investigated it in the presence of low concentrations of methylene blue and crystal violet. This study aimed to prepare and investigate the increase in TiO₂ levels in addition to the concentration of fullerene NPs (fullerene-TiO₂) as a photocatalyst

decorated with Au[11]. Peng et al. produced a series of composites by combining graphite-like C₃N₄ with C₆₀ using an in situ generation method. The resulting graphite-like C₃N₄@C₆₀ composites exhibited a considerable improvement in the efficiency of photocatalytic degradation of formaldehyde and achieved a value of 99% under visible-light exposure[12]. In this work, we attempted to evaluate the photosensitizers of the prepared films of fullerene-TiO₂ previously discussed in our previous work[13].

1. Materials and Method

For the preparation of precursors and films, all practical procedures were relied upon as referenced in our previous work; TiO₂ and Au concentrations in their colloidal forms (0.22 and 0.412 ppm, respectively) were determined via atomic absorption spectroscopy [13].

1.1. Preparation of Colloidal

TiO₂ colloidal solution was prepared by pumping their pellet with pulsed Nd: YAG laser ($\lambda = 1064\text{nm}$, 100mJ energy, 6 Hz pulse rate, 3000 pulses, and 6.67 J/cm² laser fluence). The distance between the target surfaces and laser lens is 12 cm. Next, the carbon/TiO₂ colloidal solution was prepared by irradiating carbon pellet in TiO₂ colloidal at (0, 10, 30, and 50) vol. percentage of 50 mL of distilled water (DW) using the same laser parameters as well as the same number of laser shots. A colloidal of gold nanoparticles AuNPs (with a concentration of 0.412ppm) was prepared by bombarding a piece of high-purity gold (99.999%) into 50 ml of DW employing the same laser parameters used previously but with 1000 shots.

1.2. Preparation of films

Fullerene: TiO₂ films were produced through thermal spraying of carbon colloidal solution (50 ml) on quartz glass substrates with an enhanced potential bias of 5 kV. The spraying process was carried out at a temperature of 300 ± 25 °C with a flow rate of approximately 1 ml/min (with the enhanced compressed air) and switched on and off at 10 and 30 s intervals, respectively. The distance between the nozzle and substrates was around 28 cm.

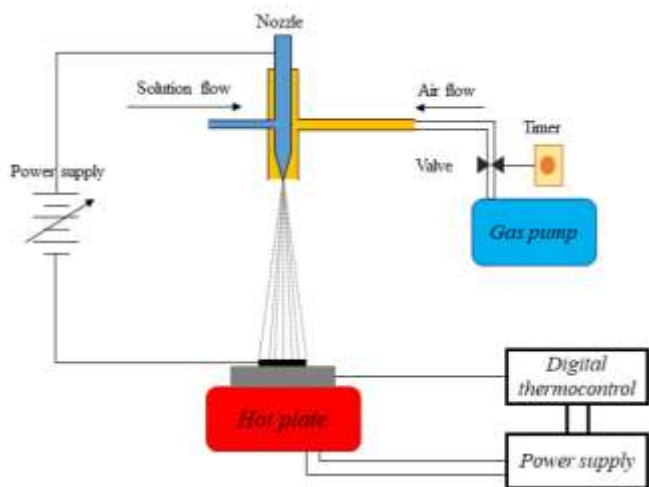


Fig.1 the setup of the used device for prepared films

1.3. Characterization:

The analysis of X-ray diffraction (XRD) patterns provided structural properties, employing X-ray $\text{CuK}\alpha$ radiation and an accelerated voltage of 40 kV. Crystalline size (D_{hkl}) was estimated based on the Williamson–Hall relation[14]

$$D_{hkl} = \left(\frac{A\lambda}{\cos\theta \cdot \beta_{hkl}} \right) + (4\varepsilon \sin\theta) \quad (1)$$

where A , λ , β_{hkl} , ε , and θ (rad) include a dimensionless shape factor (0.89), wavelength radiation of the used X-ray (0.15405 nm), full width at half maximum of the diffraction peaks, strain, and diffraction angle (radian), respectively.

Morphological properties of the prepared film surfaces were assessed through field emission scanning electron microscope (FE-SEM) images obtained with INSPECT-550. Additionally, Vibrational and rotational characteristics were determined using Raman spectra, and photoluminescence (PL) spectra were recorded. Furthermore, the photo-response was evaluated by measuring changes in electric resistance upon exposure to light in the range of 200 to 800 nm, with increments of 20 nm.

2. Result and discussion

2.1. Structural Properties

In general, XRD patterns of the prepared films showed polycrystalline systems depending on the TiO_2

presence ratios, as shown in Fig. 2. Furthermore, there is a change in the distribution of the phases, the type of dominant phase, and the crystal size according to the proportions of TiO_2 , as the films prepared without the presence of TiO_2 showed structures of fullerenes (C_{60} , C_{60} -polymer, and C_{70}) with a dominant phase of C_{60} -polymer with a crystalline size estimated at approximately 80.77 nm. While the dominant phase changed when starting by adding TiO_2 (10%) to C_{70} (600) with a size of 69 nanometers. When TiO_2 ratio was increased to 30%, C_{60} (211) appeared as the dominant phase with a size of 31.68 nm. Sequentially, with an increase in the percentage of TiO_2 to 50%, C_{70} returns to dominance, but at the (141) phase, with an increase in the crystalline size of approximately 96.7 nm. Table 1. Explains the XRD parameters of the dominate phases of the prepared films.

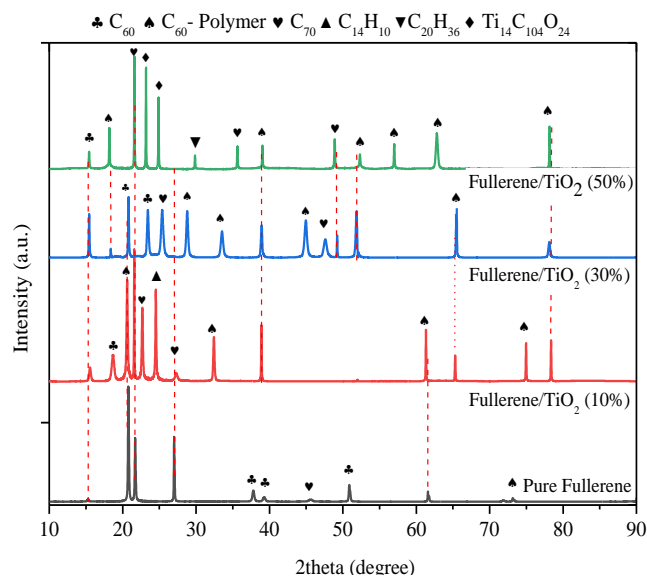


Fig. 2. XRD patterns of the prepared Fullerenes: TiO_2 films

Table. 1 XRD parameters for the dominate phases

TiO_2 Ratio	phase	hkl	crystalline size (nm)	Cryst. Syst.	Ref. Card
0%	C_{60}	3 1 1	80.77	Cubic	ICSD 98-060-2518
10%	C_{70}	6 0 0	69	Orthorhombic	ICSD 98-007-5506
30%	C_{60}	211	31.68	Cubic	ICSD 98-060-2518
50%	C_{70}	1 4 1	96.7	Orthorhombic	ICSD 98-007-5506

2.2. Raman spectroscopy

Raman spectroscopy is one of the effective techniques for characterizing carbon structures[15]. Fullerenes like C_{60} or C_{70} have high symmetry and show numerous vibrational modes, with C_{60} having ten modes and C_{70} having 53 [16]. However, in the C_{60} spectra, the apparent mean vibrational modes are $A_g^{(2)}$, $H_g^{(1)}$, $H_g^{(7)}$, and $H_g^{(8)}$ [17]. The $A_g^{(2)}$ mode is the strongest non-degenerate among the Raman-active modes, along with $H_g^{(8)}$, and has been frequently used to indicate C_{60} solids. Repeatedly, its position accurately reflects the physical state of C_{60} molecules[18]. While, $H_g^{(7)}$ is related to pentagon shear in C_{60} [19].

Raman spectra of the prepared films were measured from 0 cm^{-1} to 1800 cm^{-1} (Fig. 3). $H_g^{(1)}$ peaks dominated all the prepared films, starting at 288 cm^{-1} with free TiO_2 , but shifted to 293 cm^{-1} for 10% and 30% of the TiO_2 ratio and 295.6 cm^{-1} for 50% of TiO_2 . This location and intensity changes were due to the crystal field effect of C_{60} polymerization and increased chain length during nano peapod formation as shown in the SEM images in later discussion[20]. Meanwhile, the internal active Raman mode of the C_{60} molecule Ih polarization emerged, which is represented by $F_{2g}^{(1)}$ at a wavenumber of 640.6 cm^{-1} ; this mode fluctuated with the increase in TiO_2 ratio due to changes in the rotation factor[21]. Although the presented mode at around 900 cm^{-1} did not refer to any vibrational modes of fullerenes, it may be related to AuNPs [13]. In addition to the increase in its intensity with the TiO_2 ratio, the maximum intensity was 50 vol.% of the TiO_2 ratio at 907 cm^{-1} . This finding can be attributed to the increased abundance of TiO_2 that led to alterations in the vibration modes, especially when referring to the XRD patterns that confirmed the appearance of the phases of carbon structures other than fullerenes. Furthermore, the traumatic deterioration observed at the 1172 cm^{-1} peak is related to $T_{1u}^{(3)}$ vibrational modes in the infrared (IR) region[22]. Raman's vibrational mode of $A_g^{(2)}$ appeared at 1449 cm^{-1} ; its frequency increased with the increase in the TiO_2 content, but it declined again with the 30% and 50% increase in TiO_2 .

2.3. Morphological properties

The prepared films of fullerene: TiO_2 revealed various NP shapes dependent on the TiO_2 addition ratio, where a separation was observed between different particles, especially the rods (Fig. 4). The nanorods shown in Fig. 4a are likely to be C_{60} polymeric with an average diameter of 39 nm. The difference in the surface energy may contribute to particle separation [23]. Fig. 4b reveals the notably pronounced morphology of polymeric C_{60} in contrast to the other figures. The particles formed exhibited a resemblance to longitudinally stacked disks, with a thickness of approximately 80 nm, and interspersed spherical particles measuring approximately 34 nm as they converged toward the assembly line. Nevertheless, elevating the TiO_2 ratio to 30 and 50 vol.% led to the creation of heterogeneous aggregates with indistinct components (Figures 4c and 4d, respectively). In general, the behavior of particle assembly into the prepared films with 0, 10, and 30 vol.% exhibited fiber-like patterns.

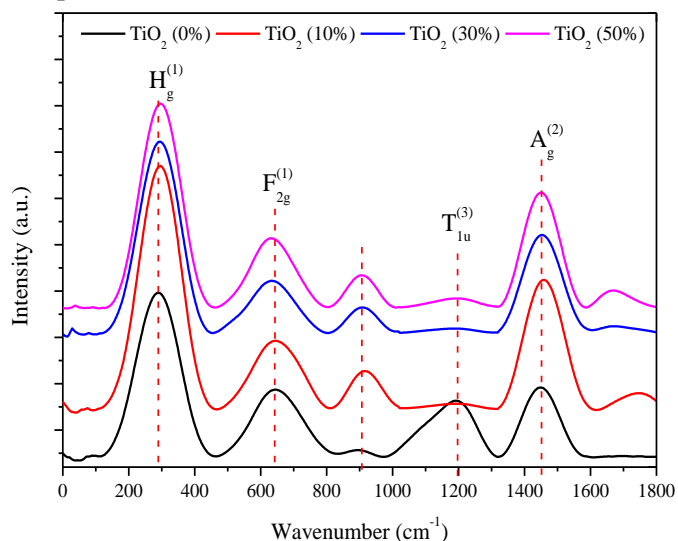


Fig. 3. Raman spectra of the prepared Fullerenes: TiO_2 films

However, the porosity varied with the change of TiO_2 ratio, where was $(53.60 \pm 0.12, 59.71 \pm 0.08, 64.13 \pm 0.15, \text{ and } 61.60 \pm 0.18)\%$. The nonlinearity in the change in porosity and the abnormality of its value at a higher ratio of titanium oxide is due to the increase in particle size and increased agglomeration, which led to

randomness and non-response to the effect of the applied electric field as was the case in previous ratios.

2.4. Photoluminescence

In semiconductors, the population of electrons can be imbalanced due to the absorption of certain light energy. This absorption causes electrons to move from lower to higher quantum states and then back down to lower states and emit photons in the process. This process is known as PL [24]. PL parameters are essential indicators for the detection of the quality and transitions and identification of point defects in semiconductors[25]. Given their electronic structure, carbonic materials, including fullerenes, exhibit unique optical and PL properties depending on the size, shape, and crystalline structure. In addition to the surrounding environment, that present at the wavelengths in the visible (Vis)–near-IR region[26]. Comprehending the PL spectra of C_{60} is a challenging task. This venture involves multiple symmetry considerations and deals with complex processes, such as Jahn–Teller distortions, which further complicate the problem. Moreover, extremely low temperatures are required to eliminate certain effects, which adds to the complexity of the task[27]. In this work, a laser with 332 nm wavelength was used to excite the prepared films. Fig. 5 illustrates the PL spectra of the prepared fullerene:TiO₂ films. The figure also reveals the spectra of the AuNP-decorated fullerene and fullerene films:TiO₂ excited at wavelengths of 280 and 320 nm. Excitation at a wavelength of 280 nm without TiO₂ addition resulted in a strong emission at the 562.2 nm line, with a red shift of 0.4 nm when TiO₂ was added (10% and 30%). Excitation at a wavelength of 280 nm without TiO₂ addition showed a strong emission at the 562.2 nm line, with a red shift of 0.4 nm when TiO₂ was added (10% and 30%). Meanwhile, those prepared with a 50% addition of TiO₂ had a shift of 0.88 nm. The emission intensity increased with the increased addition of TiO₂, which confirmed the transition to energy states below the C_{60} highest occupied molecular orbital band[5]. To detect weak emission lines, we excited the films at a wavelength of 320 nm and room temperature. The positions and intensities of the lines under UV-Vis light varied based

on the TiO₂ ratio. However, those emissions may be attributed to the $T_{1u} \rightarrow H_g$ state[26].

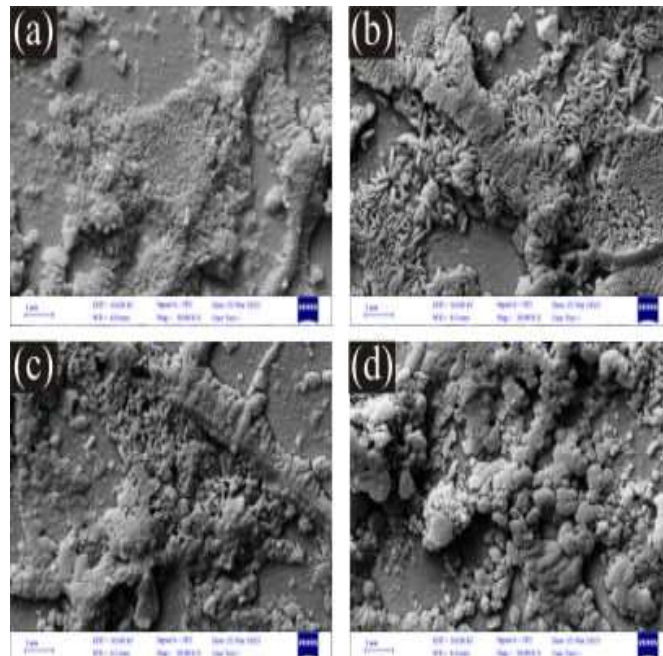


Fig. 4 SEM images of the Au-decorated Fullerene: TiO₂ films

2.5. Photoconductivity

The functioning of the Au: TiO₂: Fullerene system is based on the photoelectric conduction mechanism, as shown in Fig.6. In this system, Vis. light is absorbed by AuNPs through surface plasmon resonance (SPR), which excites the electrons. The excited electrons then cross the Schottky junction between the AuNP and the TiO₂ particles on the surface and move to the conduction band of TiO₂[28]. These electrons have the ability to move to the HUMO band, which helps in stabilizing the charge and slowing down the recombination process. These results in a longer lifespan for the free excited conduction electrons, allowing them to react with oxygen adsorbed from the surroundings. As a result, O_2^- , OH , and OOH radicals are produced, which are capable of bonding with organic groups[29,30].

To determine the optimal photoconductive behavior of the prepared films, we exposed them to monochromatic light at increments of 200–800 nm and a step of 20 nm using a tunable monochromatic light source. The current was measured with a fixed voltage

using the setup system in Fig. 7a with 10 min exposure. Fig. 7b illustrates the prepared fullerene:TiO₂ films. However, the best active wavelength was determined by graphing the incident wavelength versus average $\langle R/R_0 \rangle$, where R and R₀ denote the resistance of sample during light exposure and in the dark, respectively.

Fig. 7c shows that all fullerene films achieved the lowest value of $\langle R/R_0 \rangle$ in the visible region at around 400 nm. The $\langle R/R_0 \rangle$ value increased with the increase in the percentage of TiO₂ to 10% and 30%, and this finding may be due the absorption of light (about 500 nm) during the SPR of Au. This condition led to an abundance of electrons that shifted to the conduction band in TiO₂; these electrons then transitioned to lower energy states in fullerene's HUMO, which boosted electron lifetime and reduced compound resistance[28–30].

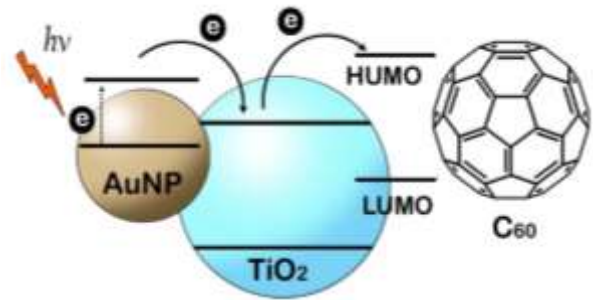


Fig.6 mechanism of the photoconduction

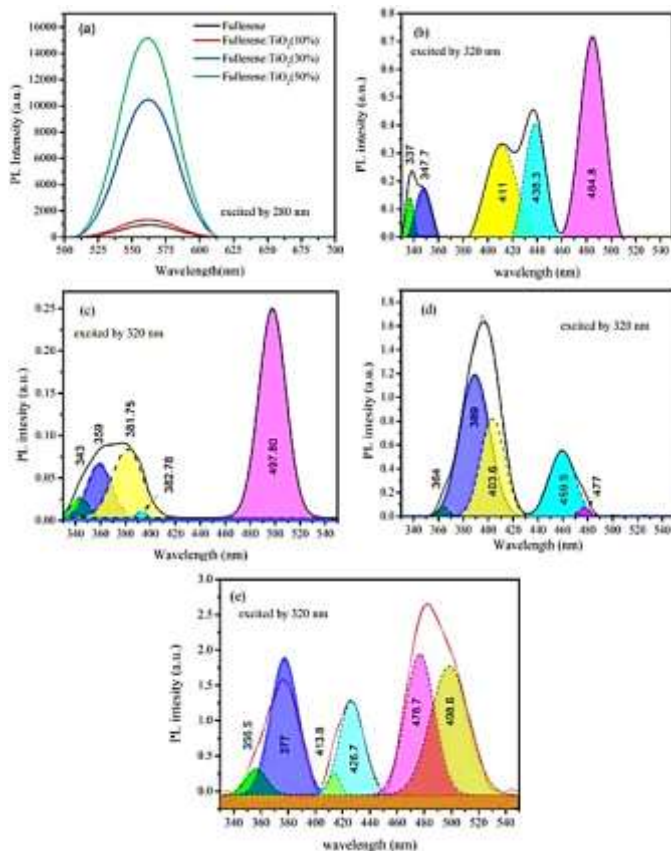


Fig.5 the PL spectra of the prepared Fullerene: TiO₂ films

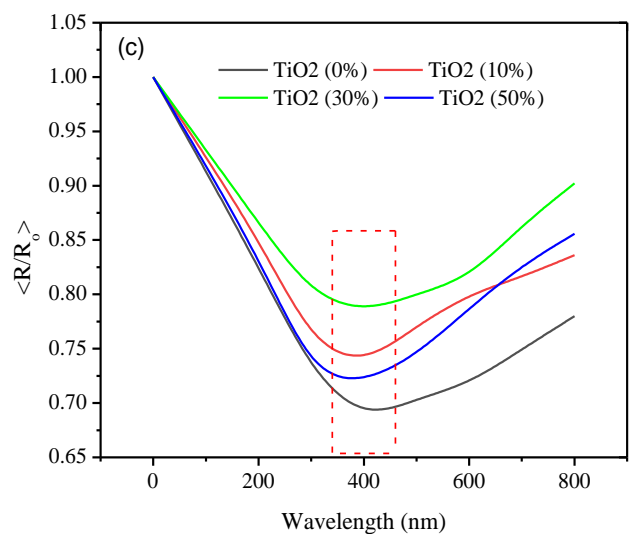
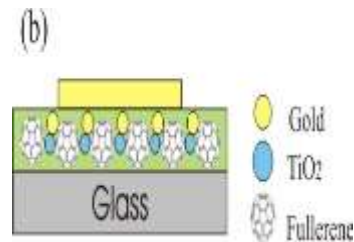


Fig.7 (a) photographic image of photodetection measuring system, (b) Au: TiO₂: Fullerene film system,

and (c) photo-behavior of the prepared Au-decorated Fullerene and Fullerene: TiO₂ films

Conclusion

Carbonic wastes can be used as one of the raw materials for the production of fullerene through inexpensive techniques. Fullerene materials possess unique properties that can be controlled through the design of energy bands. The addition of TiO₂ and Au to achieve an abundance of electrons can improve photoconductivity. However, Au-decorated fullerene: TiO₂ films showed that the vibrational modes of fullerene increased with a limited ratio of TiO₂. The PL of the films depended on the intensity of the irradiating light source and the ratio of TiO₂. Similarly, these factors affect the conduction of light within the Vis region.

References

- [1] M.R. Al-Mamun, S. Kader, M.S. Islam, M.Z.H. Khan, Photocatalytic activity improvement and application of UV-TiO₂ photocatalysis in textile wastewater treatment: A review, *J. Environ. Chem. Eng.* 7 (2019) 103248. <https://doi.org/10.1016/J.JECE.2019.103248>.
- [2] Y. Hu, Z. Xu, Application of Photocatalytic Nanomaterials in Photoelectrochemical Biosensors, *J. Phys. Conf. Ser.* 1948 (2021) 12144. <https://doi.org/10.1088/1742-6596/1948/1/012144>.
- [3] M.A. Al-Nuaim, A.A. Alwasiti, Z.Y. Shnain, The photocatalytic process in the treatment of polluted water, *Chem. Pap.* 77 (2023) 677–701. <https://doi.org/10.1007/s11696-022-02468-7>.
- [4] S. Park, Y. Keum, J. Park, Ti-Based porous materials for reactive oxygen species-mediated photocatalytic reactions, *Chem. Commun.* 58 (2022) 607–618. <https://doi.org/10.1039/D1CC04858A>.
- [5] K.I. Katsumata, N. Matsushita, K. Okada, Preparation of TiO₂-fullerene composites and their photocatalytic activity under visible light, *Int. J. Photoenergy.* 2012 (2012) 9. <https://doi.org/10.1155/2012/256096>.
- [6] and J.M. Long, Yingzhao, Yi Lu, Yan Huang, Yingchun Peng, Yanjing Lu, Shi-Zhao Kang, Effect of C60 on the photocatalytic activity of TiO₂ nanorods, *J. Phys. Chem. C.* 113 (2009) 13899–13905.
- [7] C. Feng, Z. Yu, H. Liu, K. Yuan, X. Wang, L. Zhu, G. Zhang, D. Xu, Enhanced photocatalytic performance of Au/TiO₂ nanofibers by precisely manipulating the dosage of uniform-sized Au nanoparticles, *Appl. Phys. A Mater. Sci. Process.* 123 (2017) 1–9. <https://doi.org/10.1007/s00339-017-1133-9>.
- [8] R. Vishnoi, S. Gupta, J. Bhardwaj, R. Singhal, Enhancing Non-linear Response of Fullerene via Incorporation of Gold Nanoparticles, *Plasmonics.* 15 (2020) 361–370. <https://doi.org/10.1007/s11468-019-01042-4>.
- [9] S. Qin, X. Chen, Q. Du, Z. Nie, X. Wang, H. Lu, X. Wang, K. Liu, Y. Xu, Y. Shi, R. Zhang, F. Wang, Sensitive and Robust Ultraviolet Photodetector Array Based on Self-Assembled Graphene/C 60 Hybrid Films, *ACS Appl. Mater. Interfaces.* 10 (2018) 38326–38333. <https://doi.org/10.1021/acsami.8b11596>.
- [10] X. Liu, Y. Ji, Y. Du, X. Jing, Y. Zhao, K. Dou, L. Yu, L. Chu, Q. Zhou, Mingliang Sun, A “green” all-organic heterostructure functionalized by self-assembled fullerene small molecule with enhanced photocatalytic activity, *Appl. Surf. Sci.* 585 (2022) 152738.
- [11] R. Kumar, R. Choudhary, S. Kolay, O.P. Pandey, K. Singh, P. Bhargava, Carbon coated titanium dioxide (CC-TiO₂) as an efficient material for photocatalytic degradation, *Energy Adv.* (2022) 926–934. <https://doi.org/10.1039/d1ya00015b>.
- [12] D. Peng, Z. Zhang, J. Zhang, Y. Yang, Improving Photocatalytic Activity for Formaldehyde Degradation by Encapsulating C60 Fullerenes into Graphite-like C3N4 through the Enhancement of Built-in Electric Fields, *Molecules.* 28 (2023) 5815.
- [13] H.H. Ali, M.A. Alalousi, Initial Characterization of the Prepared Au-Decorated TiO₂:Fullerene Films Using Electrospray Method, *Iraqi J. Appl. Phys.* 19 (2023) 151–156.
- [14] S. Ilyas, Heryanto, B. Abdullah, D. Tahir, X-ray diffraction analysis of nanocomposite Fe₃O₄/activated carbon by Williamson–Hall and size-strain plot methods, *Nano-Structures & Nano-*

- Objects. 20 (2019) 100396.
<https://doi.org/10.1016/j.nanoso.2019.100396>.
- [15] A.R. Shahmoradi, M.S. Bejandi, E.H. Rasanani, A.A. Javidparvar, B. Ramezanzadeh, Graphene oxide nano-layers functionalized/reduced by L-Citrulline/Pectin bio-molecules for epoxy nanocomposite coating mechanical properties reinforcement, *Prog. Org. Coatings*. 178 (2023) 107493.
<https://doi.org/10.1016/J.PORGOAT.2023.107493>
- [16] H. Chadli, F. Fergani, A. Rahmani, Structural and Vibrational Properties of C60 and C70 Fullerenes Encapsulating Carbon Nanotubes, in: N. Kamanina (Ed.), *Fullerenes Relat. Mater. Appl.*, IntechOpen, 2018: pp. 109–127.
<https://doi.org/http://dx.doi.org/10.5772/intechopen.71246> ©.
- [17] D. Jing, Z. Pan, Molecular vibrational modes of C60 and C70 via finite element method, *Eur. J. Mech. A/Solids*. 28 (2009) 948–954.
<https://doi.org/10.1016/j.euromechsol.2009.02.006>.
- [18] T. Konno, C. Hirata, E. Henrique Martins Ferreira, L. Ren, G. Piao, J. Manuel Juárez García, F. Martínez Suárez, S. Joaquín Jiménez Sandoval, T. Wakahara, K. Miyazawa, Precise Raman measurements of C₆₀ fullerene nanowhiskers synthesized using the liquid-liquid interfacial precipitation method, *Trans. Mater. Res. Soc. Japan*. 41 (2016) 289–295.
<https://doi.org/10.14723/tmrsj.41.289>.
- [19] A. Dorner-Reisel, U. Ritter, J. Moje, E. Freiburger, P. Scharff, Effect of fullerene C60 thermal and tribomechanical loading on Raman signals, *Diam. Relat. Mater.* 126 (2022) 109036.
<https://doi.org/10.1016/j.diamond.2022.109036>.
- [20] S. Samiullah, Spectroscopic characterization of fullerenes, Luleå University of Technology, 2008.
- [21] H. Kuzmany, R. Pfeiffer, M. Hulman, C. Kramberger, Raman spectroscopy of fullerenes and fullerene-nanotube composites, *Philos. Trans. R. Soc. London. Ser. A Math. Phys. Eng. Sci.* 362 (2004) 2375–2406.
<https://doi.org/10.1098/rsta.2004.1446>.
- [22] W.W. Duley, A. Hu, Fullerenes and proto-fullerenes in interstellar carbon dust, *Astrophys. J. Lett.* 745 (2012) 2008–2011.
<https://doi.org/10.1088/2041-8205/745/1/L11>.
- [23] D. Li, H. Haneda, N. Labhsetwar, S. Hishita, N. Ohashi, Visible-Light-Driven Photocatalysis on Fluorine-Doped TiO₂ Powders by the Creation of Surface Oxygen Vacancies, *Chem. Phys. Lett.* 401 (2005) 579–584.
<https://doi.org/10.1016/j.cplett.2004.11.126>.
- [24] T. Unold, L. Gütay, Photoluminescence Analysis of Thin-Film Solar Cells, in: D. Abou-Ras, T. Kirchartz, U. Rau (Eds.), *Adv. Charact. Tech. Thin Film Sol. Cells*, Second Edi, Wiley- VCH Verlag GmbH & Co. KGaA., 2016: pp. 275–297.
<https://doi.org/10.1002/9783527699025.ch11>.
- [25] M.A. Reshchikov, Measurement and analysis of photoluminescence in GaN, *J. Appl. Phys.* 129 (2021). <https://doi.org/10.1063/5.0041608>.
- [26] T.E. Saraswati, U.H. Setiawan, M.R. Ihsan, I. Isnaeni, Y. Herbani, The Study of the Optical Properties of C60 Fullerene in Different Organic Solvents, *Open Chem.* 17 (2019) 1198–1212.
<https://doi.org/10.1515/chem-2019-0117>.
- [27] A. Iwasiewicz-wabnig, Studies of carbon nanomaterials based on fullerenes and carbon nanotubes, Umeå University, 2007.
- [28] G. Panomsuwan, S. Wongcharoen, C. Chokradcharoen, M. Tipplook, O. Jongprateep, N. Saito, Au nanoparticle-decorated TiO₂ hollow fibers with enhanced visible-light photocatalytic activity toward dye degradation, *RSC Adv.* 12 (2021) 193–200. <https://doi.org/10.1039/d1ra07323k>.
- [29] J. Schneider, M. Matsuoka, M. Takeuchi, J. Zhang, Y. Horiuchi, M. Anpo, D.W. Bahnemann, Understanding TiO₂ photocatalysis: Mechanisms and materials, *Chem. Rev.* 114 (2014) 9919–9986.
<https://doi.org/10.1021/cr5001892>.
- [30] Z.Y. Wu, Y.J. Xu, L.J. Huang, Q.X. Zhang, D.L. Tang, Fullerene-cored star-shaped polyporphyrin-incorporated TiO₂ as photocatalysts for the enhanced degradation of rhodamine B, *J. Environ. Chem. Eng.* 9 (2021) 106142.
<https://doi.org/10.1016/j.jece.2021.106142>.

زحف رامان والتوصيلية الضوئية لأغشية Fullerene: TiO₂: المزيّنة بالذهب

هبة حسين علي* و مازن عبد الحميد الألوسي

جامعة الأنبار، كلية العلوم، قسم الفيزياء، الرمادي، العراق

[heb21s2007@uoanbar.edu.iq*](mailto:heb21s2007@uoanbar.edu.iq)

mazin_alalousi@uoanbar.edu.iq

الخلاصة:

تم إنشاء أغشية Fullerene:TiO₂ المزخرفة بـ Au باستخدام الرش الكهربائي بدرجة حرارة 300 درجة مئوية وجهد تحيز قدره 5 كيلو فولت. تمت دراسة الخصائص التركيبية، أطياف رامان، التلؤلؤ الضوئي، والتوصيلية كهروضوئية عن طريق تغيير نسبة TiO₂ إلى الكربون. أظهر أطياف حيود الأشعة السينية تغييراً في توزيع تراكيب C₆₀ و C₆₀ البوليمري و C₇₀. أظهرت أطياف رامان الأنماط الاهتزازية المميزة للفوليرينات (1) Hg و (1) Ag مع تغيرات طفيفة في شدة واتساع الخطوط. أظهر أطياف التآلق الضوئي تحت الإثارة عند طول موجة 280 نانومتر زيادة في شدة الذروة عند حوالي 562 نانومتر دون تغيير في موضعها. كشفت الأطياف الناتجة عن الإثارة عند طول موجي 320 نانومتر عن التحولات في منطقة Vis-UV، التي تتغير مواقعها و شدتها اعتماداً على النسبة المئوية لـ TiO₂. أدى ذلك إلى تغير في الاستجابة البصرية المقاسة بـ $\langle R/R_0 \rangle$ للأغشية المحضرة كدالة للتوصيل البصري تحت التشعيع عند الأطوال الموجية (200–800) نانومتر. و وجد أن التوصيلية الضوئية المثالية للفيلم هي Fullerene:TiO₂ (30%).

الكلمات المفتاحية: فولورين، TiO₂، التلؤلؤ الضوئي، التوصيلية الضوئية